In-situ neutron tomography and 3D numerical modeling of moisture distribution in concrete at high temperature

Dorjan Dauti

Univ. Grenoble Alpes, CNRS, Grenoble INP, 3SR, 38000 Grenoble, France,

dorjan.dauti@3sr-grenoble.fr

RÉSUMÉ. *L'écaillage est un phénomène régulièrement rencontré lorsque le béton est soumis à des températures élevées. Celui-ci expose les armatures et peut conduire à la rupture prématurée des structures telles que les tunnels, les gratte-ciels, les centrales nucléaires etc. Dans ce travail, les premières mesures 3D de la teneur en eau du béton (grandeur locale indispensable au suivi du processus de déshydratation potentiellement responsable de l'écaillage) soumis à un chargement thermique sévère ont été réalisées à l'aide de tomographies neutroniques rapides. Le suivi de la déshydratation rapide du béton a été possible en réalisant des scans 3D toutes les minutes grâce à la source neutrons de l'Institut Laue Langevin (leader mondial), à Grenoble, France. L'influence de la taille des agrégats sur la distribution de l'humidité au sein de l'échantillon est présentée. En parallèle, un modèle thermo-hydro-mécanique entièrement couplé a été mis en œuvre et utilisé pour prédire les températures et les distributions d'humidité mesurées expérimentalement. Une approche mésoscopique a également été employée dans le modèle afin d'étudier l'effet des agrégats sur le front de déshydratation.*

ABSTRACT. *One of the drawbacks of high performance concrete is its vulnerability to high temperature manifested in the form of spalling. The latter exposes the reinforcement and may lead to the premature failure of structures such as tunnels, high rise buildings, nuclear plants etc. In this communication, the first 3D measurements of moisture content in heated concrete, which is believed to be one of the processes directly related to spalling, have been performed using in-situ neutron tomography. In order to follow the fast dehydration process of concrete, one 3D scan per minute was captured thanks to the world leading flux at the Institute Laue Langevin in Grenoble France. The influence of the aggregate size on the moisture distribution is presented. A fully coupled thermo-hydro-mechanical model has been implemented and used in this study for predicting the temperature and moisture distribution measured experimentally. In addition, a mesoscopic approach is adopted in the model for investigating the effect of aggregates on the drying front.*

MOTS-CLÉS : *écaillage, déshydratation, haute température, tomographie neutron, modélisation mésoscopique*

KEY WORDS: *spalling, drying, aggregate size, high temperature, neutron tomography, mesoscale modeling*

1. Introduction

Spalling, a phenomenon encountered when concrete is exposed to high temperature, can lead to the failure of the structural element and can be a major safety hazard. Different explanations for spalling have been presented in the past. The two principal mechanisms more broadly accepted are the differential thermal gradients and the pore pressure build up. The latter is related to the evolution of the moisture content inside concrete. Studies in literature [DER 12, TOR 15] attempted the investigation of moisture distribution in heated concrete. These studies analyzed the moisture profiles in one dimension, but none of them was able to track the moisture distribution in three dimensions. Spalling is an intrinsically three dimensional process, since it locally depends on the heterogeneity of concrete. Therefore, 3D analysis is pivotal for investigating the role of aggregates in the moisture distribution in order to establish the role of the microstructure (i.e. the grain scale) in the fire response of concrete. Neutron tomography is an innovative technique which allows access to the local moisture distribution. The particularly high attenuation of hydrogen atoms makes neutron imaging a convenient method to study the moisture content (and therefore any drying front) in concrete.

This paper focuses specifically on the moisture migration in concrete exposed to high temperature, which is analyzed for the first time in 3D through *in-situ* neutron tomographies acquired at the Institute Laue Langevin (ILL) in Grenoble, France which currently has the highest neutron flux in the world. The influence of the aggregates on the moisture distribution is discussed by comparing the drying front in samples with different aggregate sizes.

On the other hand, numerical models for concrete at elevated temperature are indispensable for understanding the complex physical phenomena, particularly spalling and its mechanisms. While the existing models in literature [GAW 99, DAL 07, DAV 10] are usually validated against standard measurements of temperature, gas pressure and global mass loss [KAL 00, MIN 10] neutron imaging provides a new source of useful information to capture and account for processes occurring at the micro- and meso-scale.

A fully coupled thermo-hydro-mechanical model is implemented and used for the prediction of temperatures and moisture profiles. The esteemed numerical performance of the newly implemented code allows for running 3D simulation which is necessary for investigating the non-uniform drying front. An original mesoscopic approach is presented and validated through an experimental idealized geometry of a concrete sample with a single aggregate at the top. Such a study allows for investigating the influence of the aggregates on the drying front.

2. Neutron tomography experiment

2.1. Materials and methods

Cylindrical specimens with diameter 3 cm were tested. As one of the objectives was to see the influence of the aggregate size, two concrete mixes (see Table 1) were used: one with maximum aggregate size of 4 mm (HPC 4mm) and the other 8 mm (HPC 8mm). The overall volume of aggregates was the same for both mixes. Some of the specimens were equipped with thermocouples for temperature measurements at nominal distances 3, 10, 20 mm from the heated surface. The specimens were wrapped laterally with self-adhesive aluminium foil and placed inside a heating cell (see Figure 1a). The radiator heater placed above the sample was heated up to 500°C.

	HPC 4mm	HPC 8mm
Cement CEM I 52.5 R	488	488
Silica fume	122	122
Aggregate 0-1 mm	632.8	400
Aggregate 1-4 mm	949.2	600
Aggregate 4-8 mm	0	582
Superplasticizer SIKA 20HE	8.54	8.54
Water	189.1	189.1
w/b total	0.31	0.31

Table 1. *Concrete Mixtures*

While the sample was being heated, neutron tomography was performed (see Figure 1b). Neutron tomography is an innovative technique that can provide more detailed information about local moisture distribution. The principle of neutron tomography is very similar to x-ray computed tomography. However, in contrast to x-rays,

whose attenuation depends on the atomic number, neutrons interact with the nuclei. The hydrogen atoms of the water molecule highly attenuate neutrons, which makes possible the detection of moisture and drying front in concrete. In addition, due to the presence of free and chemically bound water, the cement paste has higher neutron attenuation than the aggregates. Thus, the latter can be easily distinguished from the cement matrix. This is not possible using x-ray source since the x-ray attenuation of aggregates and cement paste is similar.

The world leading flux at ILL allowed taking a 3D scan with 500 projections in only one minute. This time resolution was enough for capturing the fast dehydration process occurring inside concrete. In terms of space resolution, the pixel size is 200 µm. At the end of each test, higher resolution tomographies (pixel size 50 µm) have been obtained for having more details on the meso-structure as well as for determining the exact position of the embedded thermocouples which is necessary for numerical modeling. The radiographs obtained during the tests represent maps of attenuation accumulated along the neutron path through the concrete sample. In Figure 2a, one such radiograph for a given angle at a given time is reported, which highlights the portion of the sample where drying has occurred. The radiogram also shows the heater at the top. The rock wool and the aluminium are practically invisible, as by design. A 3D field of neutron radiation attenuation, as shown in Figure 2b, can be reconstructed by using a set of radiographies obtained at different angular positions. In this work, projections in 500 angular stations at regularly spaced interval between 0° to 180° are used. The reconstructions are done in the software X-act from RX Solutions. This software uses the standard Feldkamp (FDK) back projection algorithm [FEL 84]. Before the reconstruction in X-act, the recorded images have been corrected for camera electronic noise (dark current correction) and inhomogeneity of the neutron beam or of the scintillator screen (flat field correction). In addition, a selective median filter has been applied for getting rid of the dead pixels resulting from the gamma rays received by the detector.

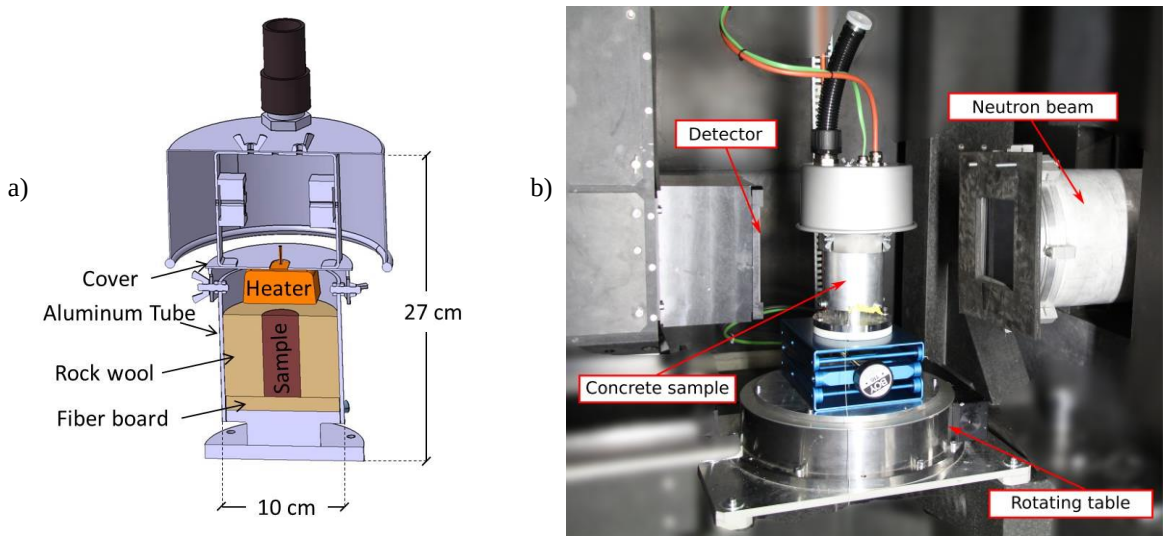

Figure 1. *Experimental setup: a) CAD drawing b) Arrangement inside the beam line at ILL*

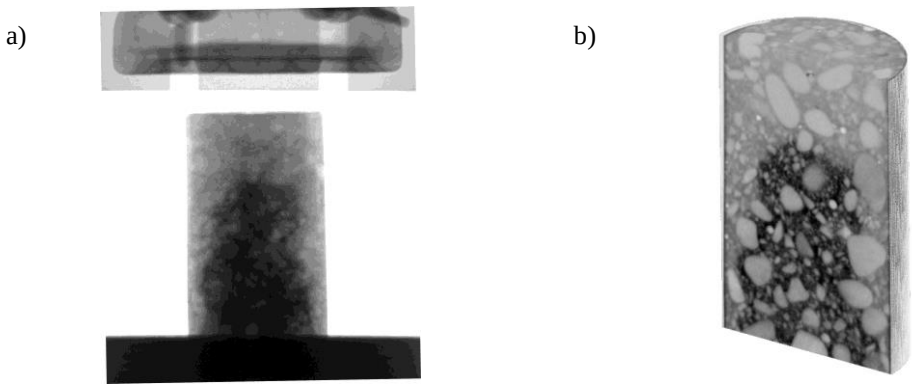

Figure 2. *a) Example of a radiogram acquired in this work b) 3D reconstruction of radiograms*

2.2. Results

In Figure 3, vertical slices from 3D scan at three different times containing the samples' axis of rotation are shown for three tested samples: HPC 8mm (left), HPC 4mm (middle), HPC 4mm with a single big aggregate at the top (right). The evolution of the drying front is evident in the images. These results show qualitatively, how the drying front moves *faster* in the sample HPC 8mm (on the left in Figure 3) compared to HPC 4 mm (on the middle in Figure 3). Another highlighted information is that, in all tested samples, there was faster drying at the lateral boundaries despite the use of heat and moisture isolation. Further image analysis has been done for a quantitative comparison of the drying front. This analysis consists on masking out the aggregates from the images for a direct comparison of the dried cement paste for each sample. Note that only the core of the sample, where the front is uniform has been considered. The results of this analysis are presented in Figure 4. HPC 8mm reaches 25 % drying, whereas HPC 4 mm only about half of it. This confirms the observation that bigger aggregates result in faster drying. The later starts when temperature at 3 mm from the surface of both samples is 170°C.

For understanding if the aggregate size has an influence on the thermal field, the temperatures measurements at three points inside each specimen are compared. The results, presented in Figure 5, show that the temperature is very similar in both samples indicating that the thermal field is not the reason behind the different drying velocity. A possible explanation of the differences in the drying front is heat induced cracking and its dependency on the aggregate size. The more pervasive fracture network induced in the HPC 8 mm would accelerate the drying process. When looking at the drying front of HPC 4 mm with a single big aggregate at the top (on the right in Figure 3), it is clear that this aggregate accelerates the drying process. Most of the acceleration of the process happens while the front is grazing the sides of the macro aggregate where the fracture network is likely to be more pervasive. This test also rules out other hypotheses, for example that the faster heat transport by the aggregate results in faster drying front, since the latter follows the sides of the aggregate and does not restart.

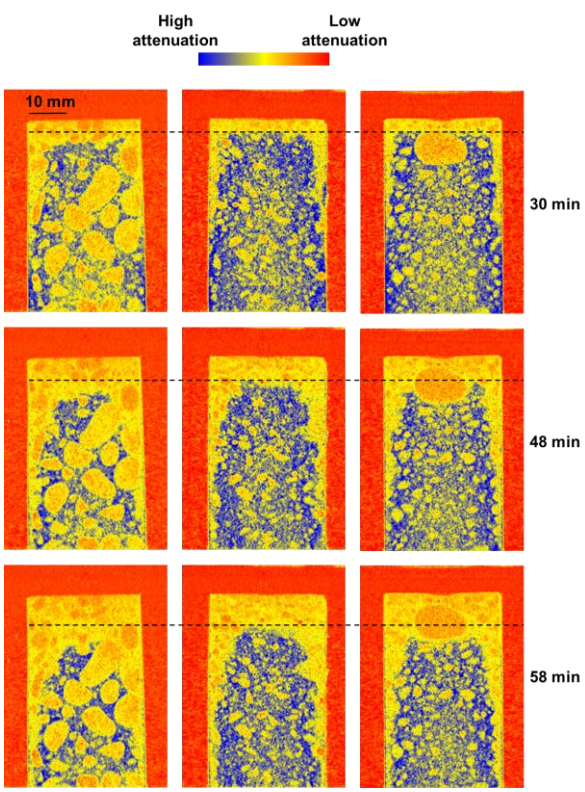

Figure 3. *Vertical slices from reconstructed 3D volumes showing the evolution of the drying front in HPC 8 mm (on the left), HPC 4 mm (on the middle) and HPC 4 mm with a single aggregate (on the right)*

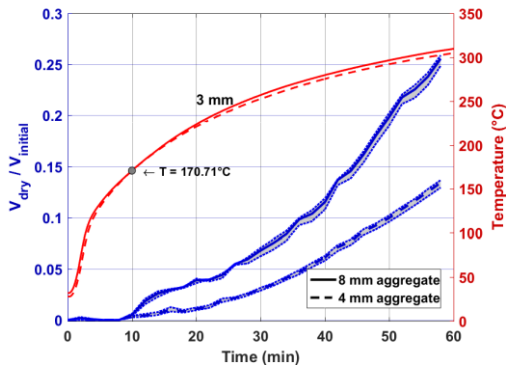

Figure 4. *Evolution of the drying front measured in terms of dry cement volume fraction considering only the core of samples HPC 8 mm and HPC 4mm*

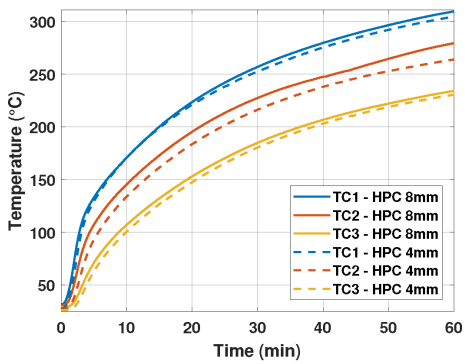

Figure 5. *Temperature profiles highlighting no difference between HPC 4 mm and HPC 8mm*

3. Numerical modeling

3.1. Mathematical model

Concrete is modeled as a porous multiphase material where the voids of the solid skeleton are filled with liquid and gas. The gas phase is considered to be a perfect mixture of dry air and water vapor. The numerical model is based on the hybrid mixture theory in the mathematical formulations proposed in [LEW 98] . For sake of brevity only the final form of the macroscopic conservation equation is given.

Dry air balance equation

$$\frac{\partial}{\partial t}(\phi(1-S)\rho_a) + \nabla\cdot\left(\rho_a \mathbf{v}_a\right) + \alpha(1-S)\rho_a \frac{\partial}{\partial t}(\nabla\cdot \mathrm{u}) = 0 \quad [1]$$

Water species (liquid-vapour) balance equation

$$\frac{\partial}{\partial t}\phi\left(S\rho_l + (1-S)\rho_v\right) + \alpha\frac{\partial}{\partial t}(\nabla\cdot \mathrm{u})\left((1-S)\rho_{gw} + S\rho_l\right) + \nabla\cdot\left(\rho_v \mathbf{v}_v + \rho_l \mathbf{v}_l\right) = \dot{m}_{\text{dehyd}} \quad [2]$$

Energy Balance equation

$$\rho c_p \frac{\partial T}{\partial t} + \nabla\cdot(-k_{\text{eff}}\nabla T) + (\rho_v c_{pv}\mathbf{v}_v + \rho_a c_{pa}\mathbf{v}_a + \rho_l c_{pl}\mathbf{v}_l)\cdot\nabla T = -\dot{m}_{\text{dehyd}}\Delta h_{\text{dehyd}} - \dot{m}_{\text{evap}}\Delta h_{\text{evap}} \quad [3]$$

where

$$\dot{m}_{\text{evap}} = \frac{\partial}{\partial t}(\phi(1-S)\rho_v) + \nabla\cdot\left(\rho_v \mathbf{v}_v\right) + \alpha S\rho_l \frac{\partial}{\partial t}(\nabla\cdot \mathrm{u}) \quad [4]$$

Linear momentum conservation equation

Linear momentum conservation equation for the mixture in terms of total stress can be written in its incremental form, neglecting inertial effects:

$$\nabla\cdot\frac{\partial\sigma}{\partial t} + \frac{\partial\rho}{\partial t}\mathbf{b} = 0 \quad [5]$$

where ρ is the averaged density of the multiphase medium given by:

$$\rho = (1-\phi)\rho_s + \phi S\rho_l + \phi(1-S)\rho_l \quad [6]$$

and $\mathbf{b}$ is the specific body force term, usually corresponding to the acceleration of gravity.

Mechanical damage effect is taken into consideration following the Mazars' scalar isotropic model [MAZ 89] combined with the thermo-chemical damage V , taking into account changes of material stiffness due to thermally induced micro cracks.

State variables are here determined in the number of 6: gas pressure p_g , capillary pressure p_c , temperature T and displacement vector of the solid matrix $\mathbf{u}\,(\mathbf{u}_x, \mathbf{u}_y, \mathbf{u}_z)$ .The balance equations are supplemented by an appropriate set of constitutive relationships which permit to reduce the number of independent state variables [DAL 07, GAW 01] . The numerical model has been implemented in the finite element software Cast3M [CEA 06] . The implemented code is 20-30 times faster than the existing implementation [DAL 07] in which the code was based on. The model has been validated against available experimental tests measuring temperature, gas pressure and mass loss [DAU 18].

3.2. Numerical Analysis

In this paper the numerical model has been used for the 3D simulations of the moisture profiles obtained through neutron tomography tests. Two case studies are considered.

3.2.1 Case Study I: Homogenized continuum

First, the simulation of temperature and moisture profiles is performed by considering the material as a homogenized continuum. The sample HPC 4 mm is considered. A cylindrical geometry has been discretized in

2mm first order tetrahedral elements. The boundary conditions have been adapted as in the experiments (see Figure 6a). For the thermal boundary condition, the heat flux on the hot side is:

$$-\mathbf{n}\cdot(-k_{\text{eff}}\nabla T) = h_T(T_{\text{ext}} - T) + \sigma\varepsilon\left(T_{\text{ext}}^4 - T^4\right) \quad [7]$$

where h_T is the convective heat transfer coefficient, σ is the Stefan-Boltzmann constant and ε is the surface emissivity and T_{ext} is the temperature of the radiant heater. On the cold side, heat convection with the ambient is considered. The effect of radiation is assumed negligible. So the heat flux is:

$$-\mathbf{n}\cdot(-k_{\text{eff}}\nabla T) = h_T(T_{\text{ext}} - T) \quad [8]$$

where the temperature T_{ext} corresponds to the room temperature. For the gas mixture, the pressure is fixed at atmospheric pressure on the hot and cold sides:

$$p_g = p_{atm} \quad [9]$$

Natural boundary condition is assumed at the lateral sides (no air flux). The boundary condition for the vapor transport through the hot and cold side is specified by the vapor flux as:

$$-\mathbf{n}\cdot(\rho_v\mathbf{v}_v + \rho_l\mathbf{v}_l) = h_g(\rho_v^{\text{amb}} - \rho_v) \quad [10]$$

where h_g is the mass transfer coefficient. The ambient vapor density is determined from the relative humidity. Faster lateral drying observed experimentally suggests a moisture leak on the sides. Therefore, same boundary condition as in Equation [10] with a lower mass transfer coefficient is adopted laterally.

Except some small discrepancies, the temperature field is well predicted (see Figure 7a). Note that the exact position of the thermoucouples (TC1, TC2 and TC3) where the temperatures are measured has been determined from the high resolution neutron images.

In the moisture profiles obtained through neutron tomography experiments, the attenuation coefficient is directly related to the water content. In numerical modeling the variation in water content (w_{change}) is calculated from the change in the saturation of pores and dehydration of cement paste:

$$w_{\text{change}} = (\phi S\rho_l)_0 - (\phi S\rho_l)_t + \Delta m_{dehyd} \quad [11]$$

The variation of the water content is normalized to the initial water content ($w_i = 189$ kg/m^3) for direct comparison with the experimental results:

$$\left|w_{\text{change}}\right| = \frac{w_i - w_{change}}{w_i} \quad [12]$$

The results of the variation of water content at different time steps are presented in Figure 7b. As in the experiments (see the results in the middle in Figure 3), a faster drying at the boundaries can be observed due to a possible moisture escape laterally. The numerical model gives also satisfactory results in terms of the speed of the drying front. In addition, a moisture accumulation (shown as darker) is observed behind the front.

3.2.2 Case Study II: Simplified mesoscopic approach

A mesoscopic approach is adopted for a simplified case of HPC 4 mm sample with a single aggregate at the top (see Figure 6b). The aggregate is modeled as a solid material (no permeability, no porosity) with a higher thermal conductivity (about 3 times) with respect to the cement paste. Thus the aggregate will transfer heat but not mass. The boundary conditions are the same as in Figure 6a.

A nonlocal damage model is used for the mechanical part [MAZ 89] . The damage parameter is coupled with the permeability of the material as in [GAW 02].

$$k = k_0 \cdot 10^{A_T(T-T_0)} \cdot \left(\frac{p_g}{p_{atm}}\right)^{A_p} \cdot 10^{A_D} \quad [13]$$

In Figure 8a the damage field is shown in the cement paste. Damage in the cement paste around the aggregate is observed due to the different thermo-mechanical behavior of aggregate and cement paste. A much higher permeability induced by the damage results in faster drying around the aggregate (see Figure 8b), as observed in the experiment (see the results in the right in Figure 3).

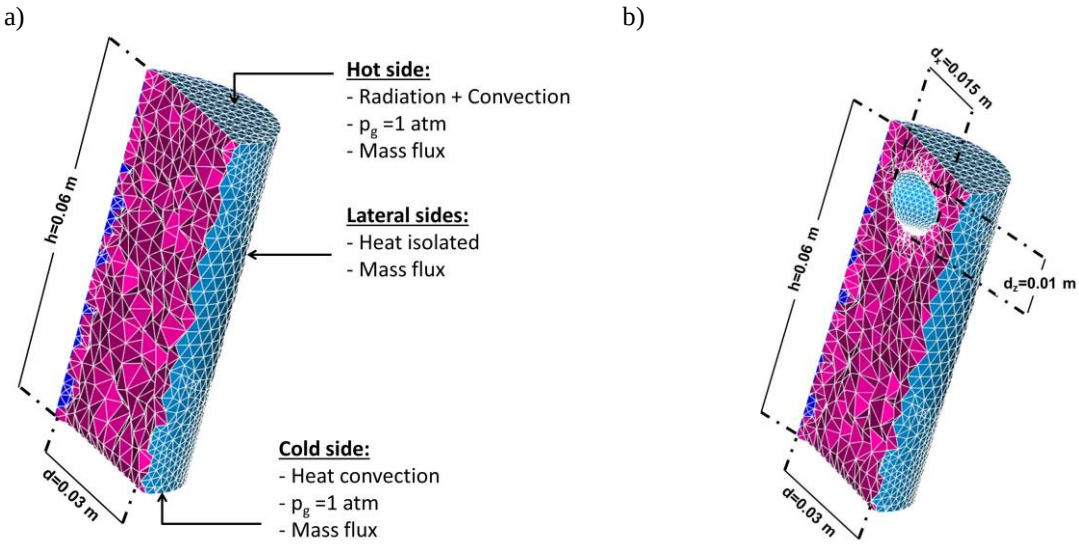

Figure 6. *Model setup showing the discretized geometry for: a) HPC 4mm (Case Study I) b) HPC 4 mm with a single aggregate at the top (Case Study II).*

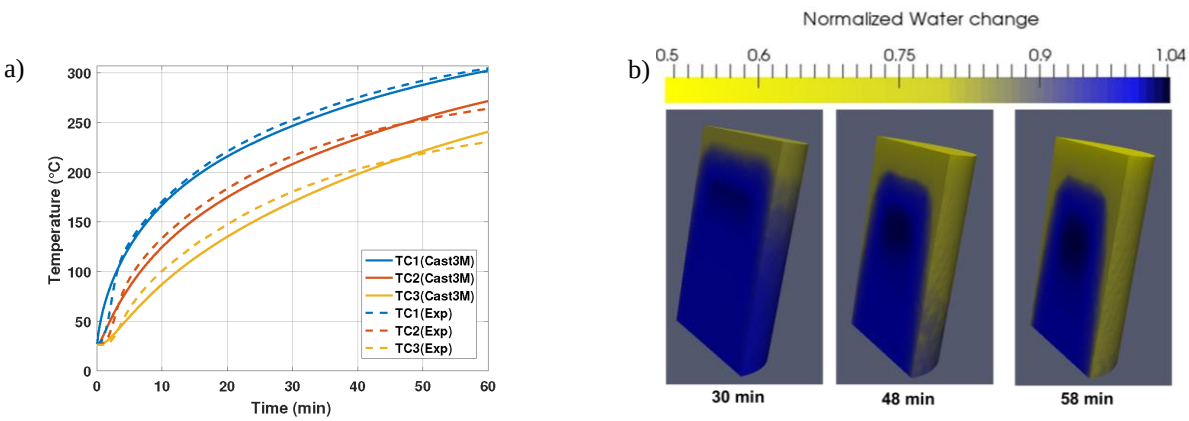

Figure 7. *Case Study I: 3D numerical simulation for predicting: a) temperature b) water content in sample HPC 4mm.*

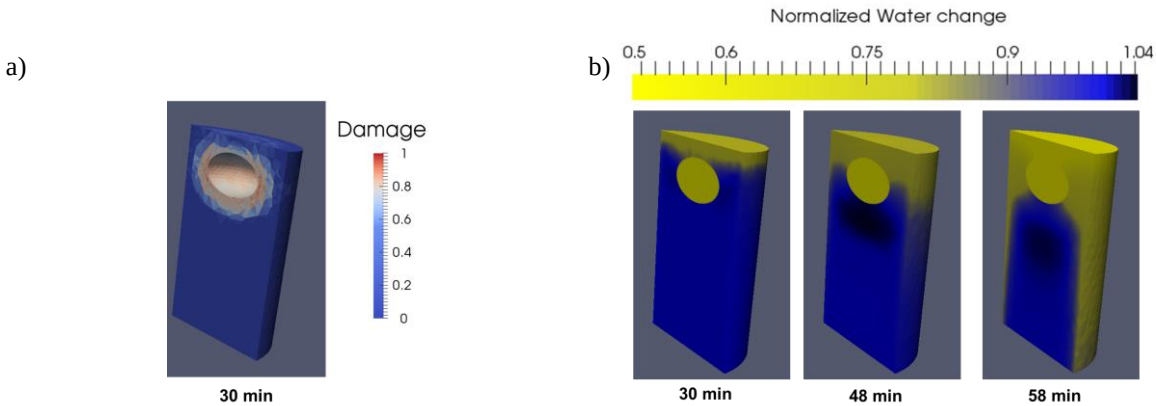

Figure 8. *Case Study II: Simulation of a) damage field and b) water content in sample HPC 4mm with a single aggregate at the top highlighting the influence of the aggregate on the moisture profile*

4. Conclusion

An experimental setup, adapted for neutron imaging and high-temperature testing of concrete has been developed. The local moisture distribution, which is believed to be directly related to spalling, has been measured for the first time in 3D by the aid of neutron tomography. Thanks to the high neutron flux at ILL it was possible to take one tomogram per minute, which is an order of magnitude faster than in other neutron tomography tests reported in the literature. The effect of the aggregate size on the global dehydration speed was investigated. Samples with 8 mm maximum aggregate size dried faster than samples with 4 mm maximum aggregate size. Results from the numerical simulations are in good accordance with the experiments in terms of temperature field, global drying speed and shape of drying front. A mesoscopic approach, adopted in the thermo-hydro-mechanical model, showed through a simplified case how an aggregate can influence the drying front. Such simulation is the first step to mesoscopic THM modeling of concrete at high temperature deemed crucial in understanding the spalling mechanisms.

5. References

[CEA 06] CEA, Cast3M, Finite element Code, CEA. 2006.

[DAL 07] DAL PONT S., DURAND S., and SCHREFLER B., «A multiphase thermo-hydro-mechanical model for concrete at high temperatures—Finite element implementation and validation under LOCA load», *Nuclear Engineering and Design*, vol. 237, 22, 2007, 2137-2150.

[DAU 17] DAUTI D., DAL PONT S., SCIUMÉ G., and BRIFFAUT M., «Numerical benchmark of experiments on heated concrete», *International Workshop on Concrete Spalling*, Borås, Sweden, 2017, 197-203.

[DAU 18] DAUTI D., DAL PONT S., WEBER B., BRIFFAUT M., TOROPOVS N., WYRZYKOWSKI M., and SCIUMÉ G., «Modelling Concrete Exposed to High Temperature: Impact of Dehydration and Retention Curves on Moisture Migration (accepted)», *International Journal for Numerical and Analytical Methods in Geomechanics*, 2018.

[DAV 10] DAVIE C.T., PEARCE C.J., and BIĆANIĆ N., «A fully generalised, coupled, multi-phase, hygro-thermo-mechanical model for concrete», *Materials and Structures*, vol. 43, 1, 2010, 13-33.

[DER 12] DER HEIJDEN G.H.A.V., PEL L., and ADAN O.C.G., «Fire spalling of concrete, as studied by NMR», *Cement and Concrete Research*, vol. 42, 2, 2012, 265-271.

[FEL 84] FELDKAMP L.A., DAVIS L.C., and KRESS J.W., «Practical cone-beam algorithm», *Journal of the Optical Society of America A*, vol. 1, 6, 1984, 612-619.

[GAW 99] GAWIN D., MAJORANA C., and SCHREFLER B., «Numerical analysis of hygro-thermal behaviour and damage of concrete at high temperature», *Mechanics of Cohesive-frictional Materials*, vol. 4, 1, 1999, 37-74.

[GAW 01] GAWIN D., MAJORANA C., PESAVENTO F., and SCHREFLER B., «Modelling thermo-hydro-mechanical behaviour of high performances concrete in high temperature environments», *Fracture Mechanics of Concrete Structures (FRAMCOS'4)*, vol. 2001, 199-206.

[GAW 02] GAWIN D., PESAVENTO F., and SCHREFLER B.A., «Simulation of damage–permeability coupling in hygro-thermo-mechanical analysis of concrete at high temperature», *Communications in Numerical Methods in Engineering*, vol. 18, 2, 2002, 113-119.

[KAL 00] KALIFA P., MENNETEAU F.-D., and QUENARD D., «Spalling and pore pressure in HPC at high temperatures», *Cement and Concrete Research*, vol. 30, 12, 2000, 1915-1927.

[LEW 98] LEWIS R.W. and SCHREFLER B.A., The finite element method in the static and dynamic deformation and consolidation of porous media, (1998).

[MAZ 89] MAZARS J. and PIJAUDIER-CABOT G., «Continuum damage theory—application to concrete», *Journal of Engineering Mechanics*, vol. 115, 2, 1989, 345-365.

[MIN 10] MINDEGUIA J.-C., PIMIENTA P., NOUMOWÉ A., and KANEMA M., «Temperature, pore pressure and mass variation of concrete subjected to high temperature—experimental and numerical discussion on spalling risk», *Cement and Concrete Research*, vol. 40, 3, 2010, 477-487.

[TOR 15] TOROPOVS N., LO MONTE F., WYRZYKOWSKI M., WEBER B., SAHMENKO G., VONTOBEL P., FELICETTI R., and LURA P., «Real-time measurements of temperature, pressure and moisture profiles in High-Performance Concrete exposed to high temperatures during neutron radiography imaging», *Cement and Concrete Research*, vol. 68, 2015, 166-173.